4th International Conference on Silicon Photovoltaics, SiliconPV 2014

Cracks in solar cell metallization leading to module power loss under mechanical loads

Jörg Käsewieter[a],*, Felix Haase[a], Marta Haro Larrodé[b], Marc Köntges[a]

[a]Institute for Solar Energy Research Hamelin (ISFH), Am Ohrberg 1, 31860 Emmerthal, Germany
[b]Department of Electrical Engineering, CIRCE Research Institute, University of Zaragoza, Maria de Luna 3, 50018 Zaragoza, Spain

Abstract

We investigate the mechanisms leading to electrically insulated cell parts in a photovoltaic module under mechanical load. For this we measure the resistances across a crack in a laminated solar cell during bending that is typical in the field. The cracks in the solar cell are detected with electroluminescence imaging. The resistance over the aluminum paste increases continuously by negligible 30 mΩ whereas the front finger resistance increases by 15.4 kΩ stepwise. This difference is the result of the higher ductility of the aluminum paste in comparison to the front finger metallization. We associate the steps in the front finger resistance measurement to breakage of single fingers with an equivalent circuit model. Furthermore we found that a silicon crack widths lower 2 µm has no influence on the resistances. Crack widths higher than 7 µm leads to a complete front finger interruption. We determine that the specific resistance of such a crack causes nearly 100% of the power loss, which is caused by a completely electrically insulating crack in a photovoltaic module.

Keywords: metallization; power loss; mechanical loads; crack width

1. Introduction

During their lifetime, photovoltaic (PV) modules are frequently exposed to mechanical loads like transport shocks, transport vibrations [1], installation loads [2], wind and snow loads. Some of these mechanical loads lead to visual defects in the module glass or the frame, but most of the damage is due to cracks in the silicon wafer of the

---

* Corresponding author. Tel.: +49-5151-999634; fax: +49-5151-999400.
  E-mail address: j.kaesewieter@isfh.de

solar cells which are not visible to the human eye. Cracks in silicon wafer material of the solar cells typically lead to only 0 % to 2.5 % power loss in standard PV modules with 60 cells [3] as long as no cell part is insulated from the bus bar by the crack. This change of power is within the uncertainty of a power measurement and therefore the damage is often not detected. However, after 15 years in the field, cells within PV modules show many insulated parts as a result of cell cracks. These cell cracks, in combination with Ethylene-vinyl acetate (EVA) browning and delamination, lead to a power loss of up to 20 % in a study by Schulze et al. with more than 250 PV modules [4]. Thus the cracks in the silicon wafer proceed to the cell metallization and insulate cell parts from the bus bar. The question is, which main processes cause the insulation in the cell metallization. The knowledge of these processes would help to assess and avoid the power loss due to cell cracks. In this work we analyze the impact of repeated mechanical loading (cycling) - comparable to wind and snow loads in the field - to the cell metallization in a mini PV module on a microscopic scale.

2. Measurements

2.1. Setup

Fig. 1 (a) shows a sketch of the 3 line bending (3LB) setup which we use to stress our mini laminate. The center positions of the bearing rolls have a distance of 9 cm and all rolls have a diameter of 1 cm. Our mini laminate has an area of 2×10 cm^2 and a 2.9 mm thick toughened float glass, 0.84 mm thick EVA double layer and 0.3 mm thick back sheet, with a 2×6.4 cm^2 part of a standard screen printed solar cell (~ 0.19 mm multi crystalline silicon and ~ 0.05 mm aluminum paste) embedded in the EVA, shown in Fig. 1 (b). This cell part consists of two 2 cm long bus bars and 9 silver fingers on the front side and full area aluminum paste on the rear side with the exception of two silver pads. In this study, we investigate the influence of cracks that form in the metal pastes, as a result of cracking in the silicon material, and we do not consider the origin of the silicon cracks. Therefore, we measure only the electrical resistance of the metal pastes following mechanical deformation. To produce a crack in the silicon material we lower the mechanical strength of the silicon by a laser perforation between the front fingers without damaging the metal pastes (1.7 mm long, 40 μm width and ~ 160 μm depth). This corresponds to possible preliminary damage of a solar cell. To additionally increase the stress on the solar cell we apply a 2 mm long and wide part of an interconnector between a front finger close to the edge and the glass, which corresponds to a bus bar. We contact each bus bar and each silver pad with a single copper ribbon (interconnector) by soldering. We guide the interconnectors through the back sheet of the mini laminate at a distance of ~ 0.3 cm from the 2 cm long edges. During bending roll displacement (d_{Br}) we measure the resistance of the front (total uncertainty = ± 20 mΩ) and rear (± 5 mΩ) side respectively with a four point resistance measurement (4PP) as shown in Fig. 1 (a) with digital multimeters 195A from Keithley (~ 1.7 mA measurement current). Our mini laminate has more than 14 cm of interconnectors for each contact outside the laminate. We correct the measured resistance values for the circuit fractions, which are outside the mini laminate and sum up all measurement uncertainties to calculate the total uncertainty (from Keithley multimeters and resistance offset measurements from circuit fractions outside of the mini laminate).
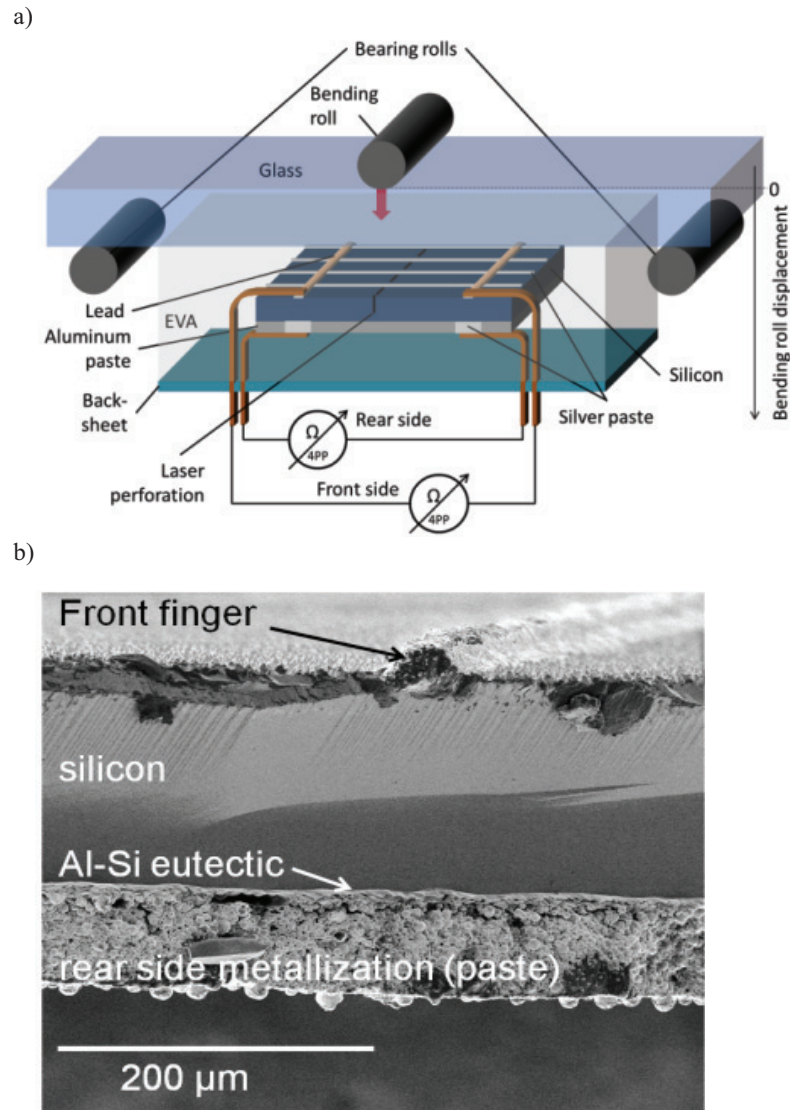
a)

b)

Fig. 1. (a) cross section sketch of mini laminate 3 line bending setup; (b) Scanning electron microscope (SEM) cross section of solar cell perpendicular to front finger.

2.2. Setup variations

For a well reproducible and automated force measurement (±0.1 N) we use the tensile testing machine BT1-FR0.5TN.D14 from Zwick with a displacement accuracy of ±10 µm, and with a bending velocity of 0.1 mm/min and an Xforce HP load cell under dark conditions. We interrupt the resistance measurement on this setup to take electroluminescence (EL) images during d_{Br}. For this we guide a current of 300 mA from the left front to the right rear side interconnector. Due to the shading of the bending setup we only observe the right half of the mini laminate front side with EL imaging. We define this setup variation as EL setup.

For crack width measurements we built a smaller setup with a micrometer screw (±20 µm) with the same 3LB boundary conditions for our mini laminate to fit into our SEM. There we can measure at the same time d_{Br}, resistances and crack width. We define this variation as SEM setup.

3. Results

3.1. Crack initiation

After lamination there is no crack in the mini laminate. We perform the first loading cycle with the EL setup. Fig. 2 (a) shows the bending force and front and rear side resistance during loading and unloading of the sample against d_{Br}. Fracturing of the sample during loading appears at ~ 0.74 mm d_{Br} and is audible. Simultaneously we measure a force drop of 3 N and an increase of ~ 15.4 kΩ of the front and ~ 15 mΩ of the rear side resistance. Discontinuous behaviors of the measurements appear every 0.1 mm d_{Br} during stopping for EL imaging. During unloading the force at the same d_{Br} is ~ 3 to 6 N lower than during loading. Furthermore, the resistances reach their initial values at ~ 0.44 mm d_{Br}. While the rear side resistance decreases continuously, the front side resistance shows discrete steps at ~ 15.4 kΩ, ~ 0.87, ~ 0.7, ~ 0.5, ~ 0.42, ~ 0.3, ~ 0.26, ~ 0.24 and ~ 0.2 Ω. Between 15.4 and 0.87 kΩ the multimeter changes the measurement range. During this change no resistance values are recorded.
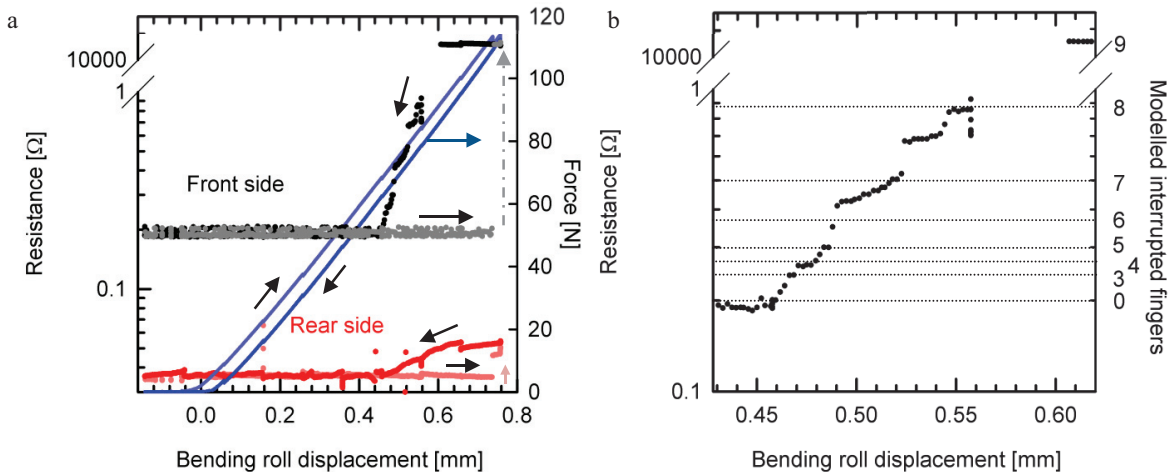

Fig. 2. (a) resistance and force measurement during first load cycle of mini laminate. The arrows show the order of the measurement; (b) enlargement of decreasing front side resistance during unloading with marked (±20 mΩ) and simulated resistance steps from model explained in 4.2.

EL images of the mini laminate during loading (Fig. 3) at 0.64 (a) and 0.74 (b) mm d_{Br} (before and after fracture) show that after the 3 N force drop, the region to the right side of laser perforation in the solar cell gets darker and the narrow left region gets brighter. If we compare EL images from 0.74 (Fig. 3 (b), nearly no intensity on right sample side) and 0.54 mm d_{Br} during unloading (Fig. 3 (c)) one brighter finger gets visible on the right sample side. The reconnected finger (4th from the top) shows an intensity (voltage potential) decrease from the crack to the bus bar. Afterwards the bus bar distributes this decreased potential to all other fingers. So the rest of the cell part is at the same voltage potential.
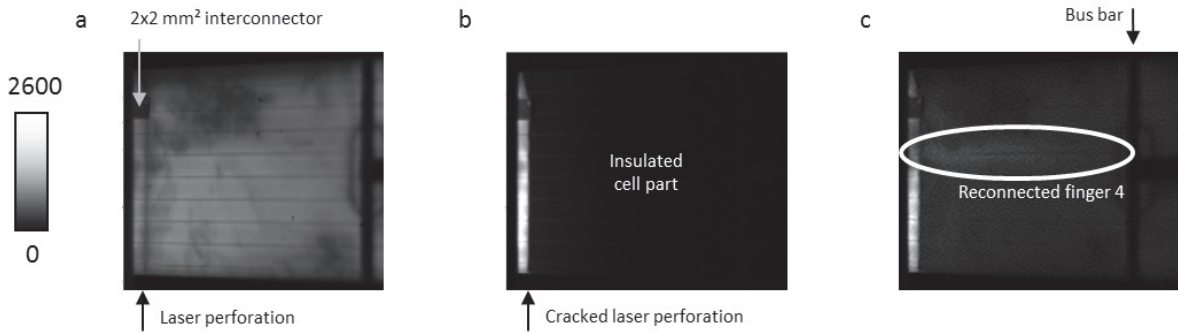
Fig. 3. EL image (a) at 0.64 mm d_{Br} (before fracture); (b) at 0.74 mm d_{Br} (after fracture); (c) during unloading at 0.54 mm d_{Br}.

After unloading, we take SEM cross section images of the mini laminate edges (see Fig. 4). In the slightly brighter silicon the crack propagates without sharp etches nearly perpendicular to the solar cell surface. This straight crack stops at the darker aluminum paste and changes to branched cracks. The cross section of the upper edge (Fig. 4(a)) shows a wider crack in the silicon and aluminum paste than at the lower edge (Fig. 4 (d)). In Fig. 4 (b) a part of the aluminum paste is clamped into the silicon crack. The crack width in the silicon at both edges is higher at the rear side than at the front side (~ 0 µm at front and ~ 2 µm at rear side).
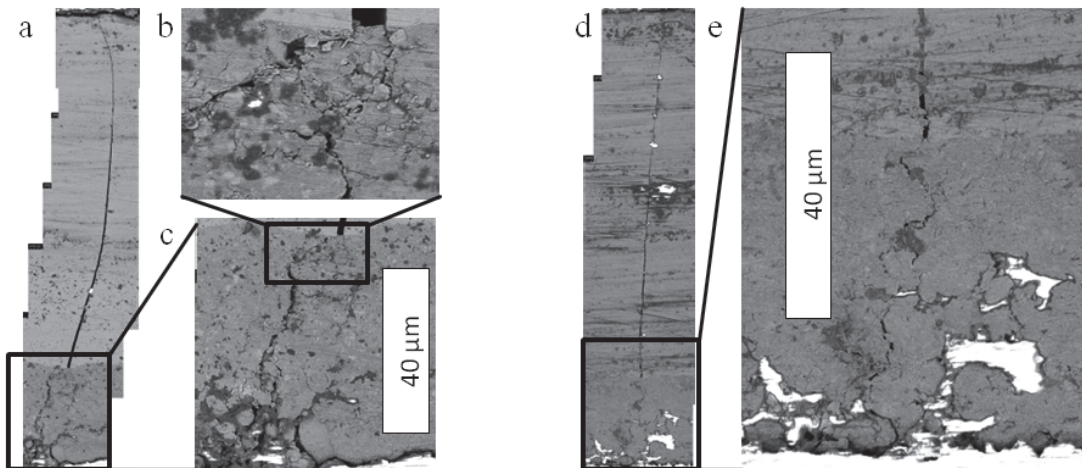

Fig. 4. SEM cross section images in unloaded sample condition of crack at: (a) upper mini laminate edge; (b) rear side interface between metal paste and silicon; (c) rear side metal paste; (d) lower mini laminate edge; (e) rear side metal paste.

3.2. Dependence of resistances on crack width

To simultaneously measure the crack width and the resistances, we use the SEM setup under an optical microscope. We bend the mini laminate up to ~ 0.29 mm d_{Br} for the fifth time after crack initiation (6th cycle). As we decrease the d_{Br} we pause every time when a change in resistances is measured. Simultaneously we take images of the crack cross section at the interface of silicon to the rear side paste (at upper edge in Fig. 4 (b)). The microscope resolution allows an uncertainty of ± 0.3 µm. In comparison to the first cycle of mechanical loading, the rear side resistance increased from 0.36 to 0.62 mΩ. During the sixth cycle the rear side resistance stays unchanged within the measurement accuracy as shown in Fig. 5 (a). As in the first cycle the front side resistance again shows discrete

steps. The first step is now at ~ 2 kΩ (~ 15.4 kΩ at crack initiation), ~ 0.7, ~ 0.42 and ~ 0.2 Ω. In comparison with the first bending cycle in Fig. 2 (a), the front side resistance decreases to its initial value at a lower displacement (0.17 instead of 0.46 mm d_{Br}) during unloading. The crack width decreases linearly from 10 μm at a d_{Br} of 0.29 mm down to 1.4 μm at a d_{Br} of ~ 0.14 mm. Below 0.14 mm d_{Br} the crack width is constant. At 0.29 mm d_{Br} the crack width shows values between 10 and 8.6 μm. This appears during a stop of ~ 68 min at a constant d_{Br}.

Fig. 5 (c) shows the dependency of the crack resistance on the crack width. The front side resistance is constant between 10 and 6.5 μm crack width. Between 6.5 and 3 μm the front resistance decreases with crack width and below 3 μm it is again constant.
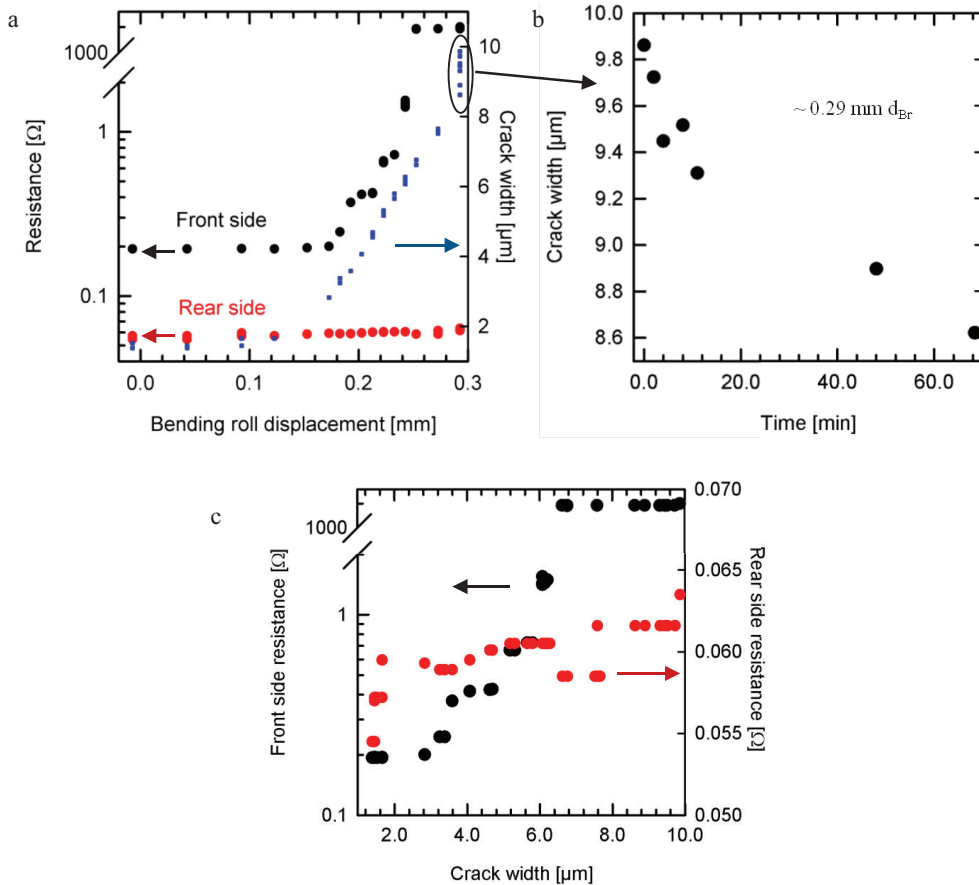

Fig. 5. (a) resistances and crack width at the upper rear side of the silicon of the mini laminate during d_{Br} with the SEM setup; (b) crack width time-evolution at 0.29 mm d_{Br}; (c) resistances of front and rear side metallization depending from rear side crack width.

4. Discussion

4.1. Viscoelastic measurement effects of EVA

Especially in Fig. 5 (b) the influence of the viscoelastic properties of the EVA [5] on the crack width is visible. While we keep the d_{Br} constant, the crack width decreases continuously over ~ 70 min by nearly 15% at room temperature. During loading (increase of strain) of the mini laminate the EVA strains the back sheet more than in equilibrium state (higher Young's modulus). If the d_{Br} is paused, the back sheet can reduce the strain due to the time dependent decreasing Young's modulus of the EVA. That results in a decrease in crack width over the time at the

same d_{Br}. During unloading (decrease of strain) we see the opposite effect; the Young's modulus of EVA is again higher than in equilibrium state. That forces the back sheet to reduce the strain more than in equilibrium. During a d_{Br} stop the back sheet can compensate for this due to the time dependent decreasing Young's modulus of the EVA, which results in an increasing crack width. The effect on the resistance measurement can be seen in Fig. 2 (a) as discontinuities in the displacement plots. During pauses in the unloading, the rear side resistance increases due to an increasing crack width. This is due to the interaction of the back sheet and the time dependent decrease of the Young's modulus of the EVA.

4.2. Current network

In Fig. 2 (b) several discrete resistance steps are observable. We develop a simple model to explain these steps. Fig. 6 shows the equivalent circuit diagram of our mini laminate. If the front fingers are fully contacted, most of the current will flow through them. But if all fingers are broken, the current flows through the pn-junction, the rear metallization and the shunt resistance. In our simulation, this current path is assumed as single ohmic resistance. Furthermore we assume an equal resistance for all 9 front fingers and a series resistance of the soldering joints and interconnectors (Offset in Fig. 6) which we subtract from the measured values. Where all 9 fingers are contacted, 0.2 Ω is assumed and 0.87 Ω (see Fig. 2 (b)) when only contact to one finger remains (see Fig. 3 (c)). That results in an offset resistance of 0.117 Ω and a single finger resistance of ~ 0.753 Ω. With a measured finger length of 5 cm and an estimated finger cross section of ~ 1000 μm² (Fig. 1 (b)) we calculate a specific resistance of 1.5 μΩcm. Hannebauer et al. calculated a value of 2.7 μΩcm [6] for a different front finger metallization. So we are in the same order of magnitude. We can distinguish 5 resistance steps with the model within the measurement uncertainty of the setup. Only the 0.7 Ω value between 7 and 8 modeled interrupted fingers cannot be explained by complete finger disruptions. This result has to be investigated in more detail.
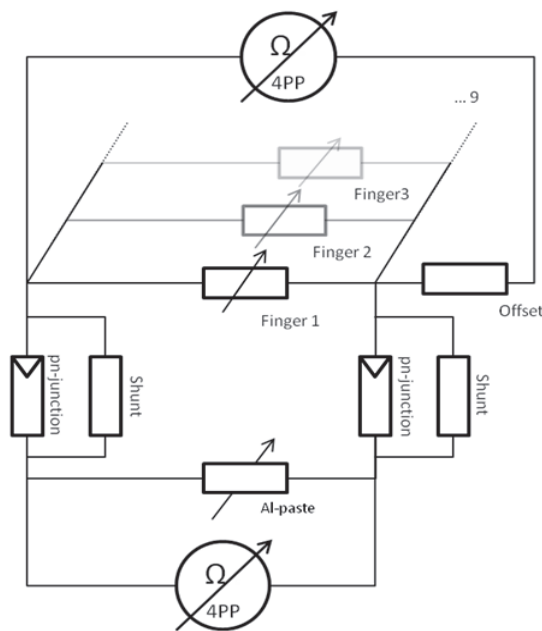

Fig. 6. equivalent circuit diagram of mini laminate for resistance measurements. Resistance steps are displayed in Fig. 2 (b), they are calculated with a single ohmic resistance instead of the pn-junction – Al-paste – shunt resistance.

4.3. Resistance behavior depending on crack width and fatigue behavior

Up to a d_{Br} of 0.14 mm the crack width is unchanged when measured within the 6th cycle (see Fig. 5 (a)). Due to the lamination and the highest thermal shrinkage of the back sheet in comparison to all other mini laminate materials, the back sheet causes compression stress in the solar cell. This compression stress has to be overcome before the crack width can increase. Front side and rear side metallization are able to compensate silicon crack widths up to ~ 2 µm without an increased resistance. Larger crack widths lead to an increase of the front side metallization resistance from 0.2 Ω to more than 2 kΩ, while the rear side metallization resistance changes only from 36 mΩ up to 62 mΩ. But in contrast to the rear side, the front fingers always return to their initial low resistance after unloading. The rear side shows fatigue that is characterized by an increase in the ground level resistance from 36 mΩ in the 1st cycle, to 56 mΩ in the 6th cycle. Furthermore, we observe the beginning of increased resistances at smaller d_{Br} with ongoing cycling of the sample (1st cycle: 0.44 mm, 6th cycle: 0.16 mm). SEM images indicate a plastic deformation of the rear side metallization (see Fig. 4 (b)) that still opens the crack without loading. Parts of the rear side metallization seem to clamp in the silicon crack. This is the reason for the higher crack width at the rear side of the silicon solar cell shown in Fig. 4 (a) in comparison to the front side crack width in Fig. 4 (d) in unloaded condition.

We simulate typical maximum curvatures in a standard photovoltaic module of 0.14 m^{-1} for 2400 Pa (IEC wind load) and 0.22 m^{-1} for 5400 Pa (IEC snow load). For such a snow load curvature we only measure crack widths larger than 20 µm in standard photovoltaic modules in a 4 line bending setup [7]. These cracks are completely insulating in the experiments.

5. Conclusion

We present an experimental setup for measuring basic parameters of the permanent power loss in PV modules. We show with our mini laminate, that a solar cell silicon fracture interrupts immediately all front fingers and deforms the rear side metallization plastically. A part of the aluminum paste is clamped in the silicon crack, which leads to a remaining crack width in the unstressed laminate of about 2 µm. As the stress on the sample is unloaded, the rear side metallization gradually returns to its initial resistance, while the front side resistance shows different discrete steps. These steps can be explained by our equivalent circuit model of our mini laminate. Furthermore, we see two different fatigue effects. The first one is that during loading the beginning of resistance increase shifts to lower bending roll displacements during 6 loading cycles. The second one is, that at the same cycling experiment the rear side metallization resistance ground level increases. Thus for the description of the crack resistance evolution two modeling approaches are needed. One model must describe the fatigue degradation of the aluminum paste depending on the number and amplitude of deformation cycles. Another model needs to describe the dependence of the front grid resistivity on the crack width (calculated from loading history of the module).

We also present a directly measured dependence of the metallization resistances to the crack width. A 2 µm crack width is compensated by both metallizations, while a crack width of ~ 7 µm interrupts all front fingers and their resistance is higher than 2 kΩ. This can be transferred to a specific resistance of 4 kΩcm. Scaling this value to a 15.6 x 15.6 cm² solar cell cracked parallel to the bus bars the crack resistance is larger than 250 Ω. As shown by Köntges et al. [3] this front side resistance causes nearly 100 % of the power loss, which is caused by a completely electrically insulating crack in a photovoltaic module. The increasing rear side resistance is neglected for this comparison.

Acknowledgements

References

[1] Köntges M, Siebert M, de la Dedicación Rodríguez A, Denz M, Wegner M, Illing R, Wegert F, Impact of transportation on silicon wafer-based PV modules, Proceedings of the 28th European Photovoltaic Solar Energy Conference, Paris, France, 2013, 4DO.2.1

[2] Olschok C, Schmid M, Haas R, Becker G, Inappropriate exposure to PV modules: description and effects of handling defaults, 28th European Photovoltaic Solar Energy Conference, Paris, France, 2013, 4AV.4.41

[3] Köntges M, Kunze I, Kajari-Schröder S, Breitenmoser X, Bjørneklett B, The risk of power loss in crystalline silicon based photovoltaic modules due to micro cracks, Sol. Energy Mater. Sol. Cells 95(4), 1131-1137 (2011)

[4] Schulze K, Groh M, Nieß M, Vodermayer C, Wotruba G, Becker G, Untersuchung von Alterungseffekten bei monokristallinen PV-Modulen mit mehr als 15 Betriebsjahren durch Elektrolumineszenz- und Leistungsmessung, Proceedings of 28. Symposium Photovoltaische Solarenergie, (OTTI, Staffelstein, Germany, 2012)

[5] Eitner U, Kajari-Schröder S, Köntges M, Altenbach H, Thermal stress and strain of solar cells in photovoltaic modules, Advanced Structured Materials 15, DOI: 10.1007/978-3-642-21855-2_29, 2011, p. 453-468.

[6] Hannebauer H, Dullweber T, Falcon T, Brendel R, Fineline printing options for high efficiencies and low Ag paste consumption, Energy Procedia 38; 2013. p. 725 – 731.

[7] Haase F, Käsewieter J, Winter R, Blankemeyer S, Morlier A, Kunze I, Köntges M, Impact of back sheet on interconnector and cell breakage in PV laminates under mechanical loads, submitted to 29th European Photovoltaic Solar Energy Conference, Amsterdam, The Netherlands, 2014.